

## Chapter 6

### Phonon induced band gap in graphene

Graphene's conspicuous lack of an electrical band gap prevents it from being used in transistor applications which require a large on/off ratio. As such, there has been a large effort to induce an electrical band gap. Groups have generated a 25 meV gap by placing graphene on hexagonal boron nitride breaking the A, B sub-lattice symmetry (Hunt et al., 2013), generated a tunable gap of up to 250 meV by applying an out-of-plane electrical field to bilayer graphene (Zhang et al., 2009), and theorists have predicted that electron confinement in graphene nanoribbons should generate a bulk band gap (Castro Neto et al., 2009). Iadecola and co-workers recently proposed an alternative, dynamic method of gapping graphene (Iadecola et al., 2013a; Iadecola et al., 2013b). They showed that when graphene is pushed out of equilibrium by exciting a particular optical phonon, the electrical band structures exhibit gaps.

In this chapter we consider the effects of these distortions in the frame work of a Peierls transition and discuss the prospects of measuring the induced band gap. This discussion represents the opposite limit of Chapters 3 and 5 where the effect of long wavelength lattice distortions on graphene's electrical and thermal properties were discussed.

## 6.1 Theory

In <sup>1</sup> This section briefly discusses Iadecola and coworker's theory of the phonon induced band gap in graphene <sup>using</sup> in the framework of a Peierls transition. Although the real space approach is slightly different, the results are in agreement with Iadecola and coworkers.

When considering how these phonon modes affect the electronic dispersion, we will use the Born-Oppenheimer approximation. According to this approximation, the very fast electrons react nearly instantaneously to the slow, phonon induced modifications of the lattice. This allows the modified electronic dispersion to be calculated assuming the lattice is frozen in sequential snapshots. In this section this calculation is done using a tight binding model in the expanded unit cell of the deformed lattice. It is performed in two parts. First, the effects of the change in lattice periodicity are discussed including a discussion of the zone folded electrical dispersion. Second, it is shown that by perturbing the zone folded Hamiltonian, the phonons gap the electronic dispersion.

### 6.1.1 The Kekulé phonon

The phonon which induces the electrical band gap is the so-called Kekulé phonon (Hou et al., 2007), the highest energy optical phonon at the  $\mathbf{K}$  point. Displacement vectors describe the eigenmode of this phonon by detailing the displacements of the atoms in the A and B sub-lattices originally at position  $\vec{r}_{A,B}$

$$u^{A,B}(\vec{r}_{A,B}, t) = \frac{1}{2} c e^{i\vec{r}_{A,B} \cdot \mathbf{K}} e^{-i\omega t} \begin{pmatrix} 1 \\ \mp i \end{pmatrix} + \text{c.c.}, \quad (6.1)$$

where the top sign corresponds to the A sub-lattice and the bottom sign corresponds to the B sub-lattice. Here  $c$  is the amplitude,  $\omega$  is the frequency of the phonon, and  $t$  is time. Snapshots showing the time dependence of the resulting lattice distortion are shown in Figure 6.1. The atoms in each sub-lattice rotate around their equilibrium positions without ever returning to their equilibrium position. Atoms in the A sub-lattice are left handed, rotating in the clockwise direction while the atoms in the B sub-lattice are right handed. At  $\omega t = \{90^\circ, 210^\circ, 330^\circ\}$  adjacent A and B sub-lattice atoms form well ordered dimers with their nearest neighbors. In the intervening time the system remains partially dimerized. This dimerization is similar to the Peierls distortion in polyacetylene except that in this two dimensional analog the system does not gap spontaneously. Instead the phonon must be continuously excited to maintain the gap. *in graphene.*

The time reversed pair of the  $\mathbf{K}$  Kekulé phonon, the  $\mathbf{K}'$  Kekulé phonon exhibits a similar distortion with sub-lattices rotating with opposite handedness. The resulting electrical dispersion is the same for either mode so for simplicity we concentrate only on the  $\mathbf{K}$  phonon. However, if both  $\mathbf{K}$  and  $\mathbf{K}'$  modes are excited simultaneously, the opposite circular polarizations sum to linear polarized atomic motion with only temporary dimerization and no sustained band gap. Thus, the experimental realization of this effect requires the exclusive excitation of the  $\mathbf{K}$  or the  $\mathbf{K}'$  Kekulé phonon.

### 6.1.2 Kekulé geometry

The Kekulé distortion causes an expansion of the unit cell, a reduction of the BZ, and a modification of the primitive lattice vectors and reciprocal lattice vectors. When referencing this new geometry back to graphene's intrinsic geometry, the notation previously developed in Chapter 2 is used. The expanded periodicity of the Kekulé lattice is determined by the periodicity of the distortion in Equation 6.1. This term

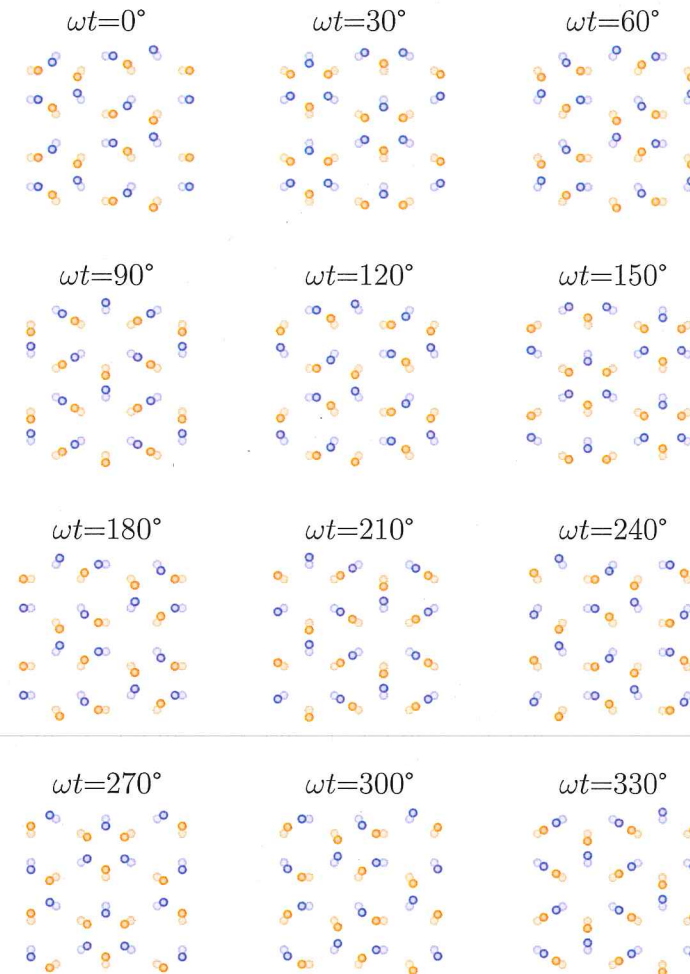


Figure 6.1: Snapshots of the Kekulé phonon mode spanning one period of oscillation. The A sub-lattice is in orange and the B sub-lattice in blue. Faded dots indicating the intrinsic graphene lattice are included for reference.

pretty!

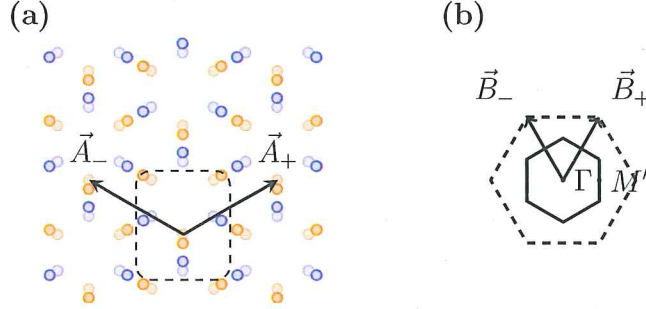


Figure 6.2: The real space (a) and reciprocal space (b) geometry of the Kekulé lattice. (a) shows a snapshot of the atomic positions with the A sub-lattice in orange and the B sub-lattice in blue. For reference, the intrinsic graphene lattice is shown using faded dots. The dashed rectangle outlines the time independent unit cell and the labeled arrows represent the primitive lattice vectors. In (b) the dashed hexagon indicates the BZ of intrinsic graphene while the hexagon with solid lines indicates the shrunken BZ of the Kekulé lattice. The primitive reciprocal lattice vectors are labeled along with select high symmetry points.

repeats whenever

$$2\pi = \vec{r}_{A,B} \cdot \mathbf{K} = (m\vec{a}_+ + n\vec{a}_-) \cdot (\vec{b}_+ - \vec{b}_-)/3 = \frac{2\pi}{3}(m-n) ,$$

where  $m$  and  $n$  are integers. Thus, at any snapshot in time the electrons see the expanded six atom unit cell shown in Figure 6.2. This tripled unit cell is time independent; it never returns to the intrinsic two atom basis.

The primitive lattice vectors of the Kekulé lattice,

$$\begin{aligned}\vec{A}_+ &= 2\vec{a}_+ - \vec{a}_- = \frac{3a}{2}(+\sqrt{3}, 1) \\ \vec{A}_- &= 2\vec{a}_- - \vec{a}_+ = \frac{3a}{2}(-\sqrt{3}, 1) ,\end{aligned}$$

represent a triangular lattice rotated by 90 degrees and expanded by a factor of  $\sqrt{3}$  relative to the intrinsic lattice. This tripling of the area of the unit cell is accompanied by a corresponding decrease in the area of the BZ as shown in Figure 6.2. The primitive reciprocal lattice vectors,

$$\vec{B}_+ = \frac{1}{3}(2\vec{b}_+ + \vec{b}_-) = \frac{2\pi}{3\sqrt{3}a}(+1, \sqrt{3})$$

$$\vec{B}_- = \frac{1}{3}(2\vec{b}_- + \vec{b}_+) = \frac{2\pi}{3\sqrt{3}a}(-1, \sqrt{3}),$$

generate a hexagonal BZ rotated 90 degrees with ~~area condense~~ shrunk by a factor of three relative to the intrinsic lattice. Unlike for intrinsic graphene, the interesting physics occurs near the center of the BZ. For completeness, three equivalent corners of the BZ are positioned at

$$\frac{2\pi}{9a}(-\sqrt{3}, -1), \quad \frac{2\pi}{9a}(+\sqrt{3}, -1), \quad \text{and} \quad \frac{2\pi}{9a}(0, 2).$$

Hence, the periodicity of the phonon fully describes the geometry of the expanded lattice.

### 6.1.3 Zone folding

When the BZ is reduced in size, the number of bands in the electronic dispersion is increased. Energy bands outside the new BZ are folded into the new BZ by translation by reciprocal lattice vectors. Since the size of BZ is reduced by a factor of three, there are two zone folding schemes resulting in six energy bands.

The zone folding schemes shown in Figure 6.3 describe the two distinct ways the symmetry reduced area of the new BZ can be mapped onto via translations of reciprocal lattice vectors. The rest of the BZ can be constructed using symmetry

(a) Zone Fold 1      (b) Zone Fold 2

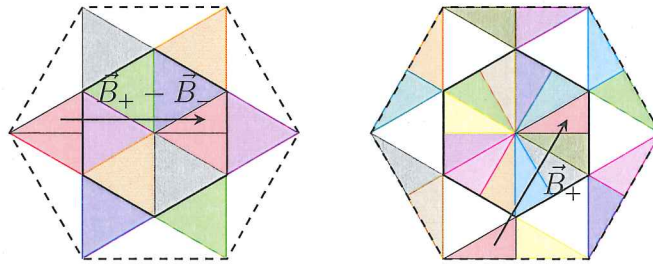


Figure 6.3: The zone foldings introduced by the Kekulé distortion. The outer, dashed hexagon is the BZ of intrinsic graphene and the inner hexagon with solid lines is the new BZ of the Kekulé lattice. The symmetry reduced area represented by the black outlined triangle is translated into the new BZ by different reciprocal lattice vectors (labeled) for the two folding schemes. *introduce (a) & (b) in caption.*

operations on the symmetry reduced area. In both zone folding schemes, the Dirac point is translated from the corner of the old BZ to the zone center of the new BZ making the  $\Gamma$  point the most interesting point in the new BZ. It is also worth noting that the right edge of the symmetry reduced area in zone fold 1 shares its right edge with the symmetry reduced area already inside the new BZ. Also, the top edge of the symmetry reduced area is shared between zone fold 1 and zone fold 2.

The hierarchy of the folded energy bands can be determined by comparing the zone folded areas to the electronic dispersion of intrinsic graphene shown in Figure 2.2. The lowest and highest energy bands will correspond to the unfolded area because the new BZ occupies the basin in the intrinsic graphene dispersion. Zone fold 1 extends further into the basin of intrinsic graphene's dispersion than zone fold 2 and so gives the second lowest and second highest energy bands. Finally, the zone fold 2 gives the two middle energy bands.

The zone folded electronic dispersion can either be calculated by folding the dispersion calculated in Chapter 2 or by performing a tight binding calculation in the expanded unit cell. Although it is more involved, the tight binding calculation will be done here because it will be needed later. In this scheme, each of the six atoms in the unit cell must have its own raising and lowering operator. To simplify this bookkeeping the operators will be referenced back to the three two-atom-bases which make up the six-atom Kekulé basis. These two-atom-bases are shown in Figure 6.4. The operators  $a_{i,l}$  and  $b_{i,l}$  are then the lowering operators for the three A sub-lattice atoms and the three B sub-lattice atoms in the  $l$ th Kekulé basis respectively. The index  $i$  run over the three two atom bases. In this notation the real space nearest neighbor tight binding Hamiltonian is given by

$$\begin{aligned} H = - \sum_l & (ta_{1,l}^\dagger b_{1,l} + ta_{1,l}^\dagger b_{2,l} + ta_{1,l}^\dagger b_{3,l} \\ & + ta_{2,l}^\dagger b_{1,l\uparrow} + ta_{2,l}^\dagger b_{2,l} + ta_{2,l}^\dagger b_{3,l\leftarrow} \\ & + ta_{3,l}^\dagger b_{1,l\uparrow} + ta_{3,l}^\dagger b_{2,l\leftarrow} + ta_{3,l}^\dagger b_{3,l} + \text{H.C.}) . \end{aligned} \quad (6.2)$$

Later the hopping energies  $t$  will be made bond dependent to account for the altered nearest neighbor distances. In the meantime the bond independent hopping energy of intrinsic graphene,  $t_0$ , will be used.

Similarly to intrinsic graphene, the individual terms in the sum can be simplified by writing the operators in Fourier space,

$$a_{m,l}^\dagger = \frac{1}{\sqrt{N}} \sum_{\vec{k}} e^{i\vec{k}\cdot\vec{R}_l} a_{m,\vec{k}}^\dagger , \quad (6.3)$$

where we are expanding about the positions of the Kekulé unit cells. The individual

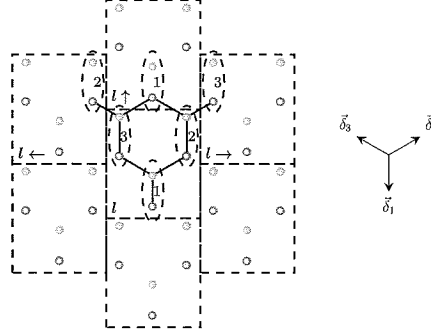


Figure 6.4: The hoppings included in the Hamiltonian connect atoms originally from the A sub-lattice (orange) to atoms originally from the B sub-lattice (blue). They can pass between the labeled intrinsic unit cells (dashed ellipses) and they can also pass between the labeled extended unit cells (dashed rectangles). For reference the directions of the nearest neighbor vectors are included.

terms are then

$$\begin{aligned}
 -t_0 \sum_l a_{m,l}^\dagger b_{m',l'} &= -\frac{t_0}{N} \sum_l \sum_{\vec{k}, \vec{k}'} a_{m,\vec{k}}^\dagger b_{m',\vec{k}'} e^{i\vec{R}_l \cdot (\vec{k} - \vec{k}')} e^{i(\vec{R}_l - \vec{R}'_l) \cdot \vec{k}'} \\
 &= -t_0 \sum_{\vec{k}} a_{m,\vec{k}}^\dagger b_{m',\vec{k}} \underbrace{e^{i(\vec{R}_l - \vec{R}'_l) \cdot \vec{k}'}}_{s_{l-l'}} ,
 \end{aligned}$$

which is only dependent on the  $l$  independent distance  $l - l' \in \{0, \leftarrow, \uparrow, \rightarrow\}$  between the Kekulé unit cells that are being hopped between.

The Hamiltonian can then be expressed in matrix form as

$$H_0 = -t_0 \sum_{\vec{k}} \psi^\dagger \begin{pmatrix} 0 & 0 & 0 & s_0 & s_0 & s_0 \\ 0 & 0 & 0 & s_\uparrow & s_0 & s_\rightarrow \\ 0 & 0 & 0 & s_\uparrow & s_\leftarrow & s_0 \\ s_0^* & s_\uparrow^* & s_\uparrow^* & 0 & 0 & 0 \\ s_0^* & s_0^* & s_\leftarrow^* & 0 & 0 & 0 \\ s_0^* & s_\rightarrow^* & s_0^* & 0 & 0 & 0 \end{pmatrix} \psi , \quad (6.4)$$

where  $\psi^\dagger = (a_1^\dagger, a_2^\dagger, a_3^\dagger, b_1^\dagger, b_2^\dagger, b_3^\dagger)$ . The six by six Hamiltonian will provide six energy levels as expected.

*6x6*

The resulting electronic dispersion is shown in Figure 6.5. To best show the shapes of the bands the dispersion is plotted both over the full Kekulé BZ and also over only the symmetry reduced area. The six energy bands are clearly visible with the highest and lowest energy bands appearing as caps. As expected the Dirac point has been shifted to zone center where the four middle bands converge to touch at a single point. In agreement with the zone folding schemes the highest energy band is degenerate with the second highest energy band on the BZ border. Also, the second and third highest energy bands are degenerate along the lines connecting the  $\Gamma$  point to the corner of the BZ. The electronic dispersion calculated with a tight binding model of the expanded unit cell agrees with our zone folding predictions.

#### 6.1.4 Altered hoppings

The excitation of the Kekulé phonon mode does more than just enlarge the unit cell, it also modifies the hopping energies. This is similar to the case of strained graphene where the altered bond lengths caused altered hopping energies and generated new

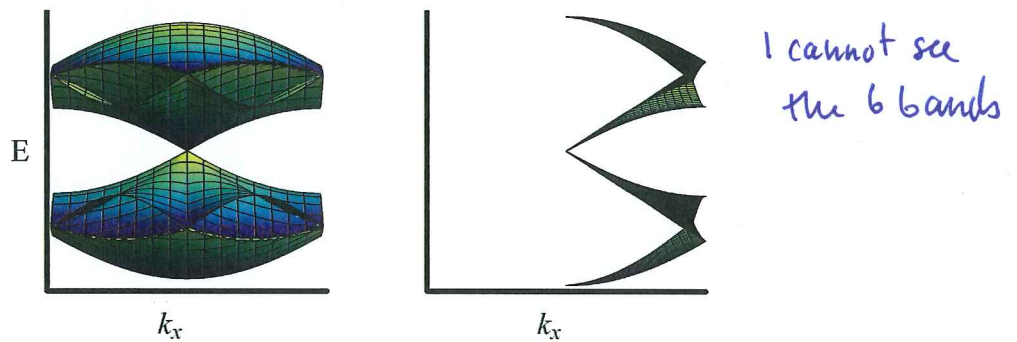


Figure 6.5: Surface plots of the folded electronic dispersion of the Kekulé lattice including all six energy bands. In the left plot the surfaces are plotted for the full Kekulé BZ whereas in the right plot only the symmetry reduced area is plotted.

physics. In this case, however, the bond lengths vary with a much higher spatial frequency and the slowly varying approximation described in Appendix B is not applicable. This coupling will generate a band gap at the  $\Gamma$  point of the zone folded dispersion.

Iadecola *et al.* showed that the bond length alterations generate hopping alterations,

*not the new  $\vec{B}$  vectors?*

$$\delta t_{m,j} = \frac{1}{3} \Delta(t) e^{i\mathbf{K} \cdot \vec{\delta}_j} e^{i\mathbf{G} \cdot \vec{r}_m} + \text{c.c.}$$

with  $\Delta(t) = -i3\beta t_0 \frac{c^*}{a} e^{i\omega t}$ , (6.5)

which have a spatial frequency component of  $\mathbf{G} = \mathbf{K} - \mathbf{K}'$  that couples the Dirac points (Iadecola *et al.*, 2013a). Here  $\vec{r}_m$  is the position of the A sub-lattice atom involved in the hopping. Index  $m$  indicates which of the three intrinsic unit cells embedded in the enlarged Kekulé unit cell the atom is in. The B sub-lattice atom is specified through  $\vec{\delta}_j$ , the unperturbed nearest neighbor vector which connects the A

sub-lattice atom to the B sub-lattice atom. Figure 6.4 summarizes these indices. For completeness, the calculation of Equation 6.5 is included in Appendix E. It is worth noting that the Cauchy-Born rule cannot be used here as it was in Section 3.1.2. *because...*  
 The iTO phonon causes the atoms in the A and B sub-lattices to rotate in opposite directions, an effect which is not captured in the Cauchy-Born frame work.

### 6.1.5 Tight binding of the expanded Kekulé lattice

The Kekulé mode causes the hopping energies in Equation 6.2 to be bond and time specific. Taking  $t = t_0 + \delta t_{m,j}$  with  $\delta t_{m,j}$  defined in equation 6.5 breaks Equation 6.2 into two pieces. The first, corresponding to  $t_0$ , is just the zone folding Hamiltonian in Equation 6.4. The second is the perturbation which opens the band gap.

Similar to the individual terms in  $H_0$ , each term in the perturbed Hamiltonian,  $H'$ , can be simplified by writing the operators in Fourier using Equation 6.3

$$\begin{aligned} -\delta t_{m,j} \sum_l a_{m,l}^\dagger b_{m',l'} &= -\frac{\delta t_{m,j}}{N} \sum_l \sum_{\vec{k}, \vec{k}'} a_{m,\vec{k}}^\dagger b_{m',\vec{k}'} e^{i\vec{R}_l \cdot (\vec{k} - \vec{k}')} e^{i(\vec{R}_l - \vec{R}'_l) \cdot \vec{k}'} \\ &= -\sum_{\vec{k}} a_{m,\vec{k}}^\dagger b_{m',\vec{k}} \underbrace{\delta t_{m,j} e^{i(\vec{R}_l - \vec{R}'_l) \cdot \vec{k}}}_{g_{m,j,l-l'}}. \end{aligned}$$

In addition to the  $l$  independent distance between involved Kekulé unit cells, each term depends on  $m$  which indicates the old, two atom unit cell which the A sub-lattice atom occupies, and  $j$  which indicates which  $\vec{\delta}_j$  the hopping is along. The associated vectors are  $\vec{R}_l - \vec{R}'_l \in \{0, \vec{A}_+, \vec{A}_+ + \vec{A}_-, \vec{A}_-\}$  and  $\vec{r}_m \in \{0, \vec{a}_+, \vec{a}_-\}$ .

The perturbed Hamiltonian can then be constructed using Figure 6.4,

$$H' = -\frac{1}{3} \sum_{\vec{k}} \psi^\dagger \begin{pmatrix} 0 & 0 & 0 & g_{1,1,0} & g_{1,2,0} & g_{1,3,0} \\ 0 & 0 & 0 & g_{2,3,\uparrow} & g_{2,1,0} & g_{2,2,\rightarrow} \\ 0 & 0 & 0 & g_{3,2,\uparrow} & g_{3,3,\leftarrow} & g_{3,1,0} \\ g_{1,1,0}^* & g_{2,3,\uparrow}^* & g_{3,2,\uparrow}^* & 0 & 0 & 0 \\ g_{1,2,0}^* & g_{2,1,0}^* & g_{3,3,\leftarrow}^* & 0 & 0 & 0 \\ g_{1,3,0}^* & g_{2,2,\rightarrow}^* & g_{3,1,0}^* & 0 & 0 & 0 \end{pmatrix} \psi .$$

Using the Born-Oppenheimer approximation the electronic dispersion of the total Hamiltonian,  $H = H_0 + H'$ , can now be calculated at any snapshot in time. In this approximation it turns out that the dispersion is time independent. Figure 6.6 shows the electronic dispersion along the  $\Gamma$  to  $M'$  direction for a lattice distortion of  $c^*/a = 1\%$ . It is clear that the modified hoppings which couples the  $\mathbf{K}$  point to the  $\mathbf{K}'$  point opens a band gap at the charge neutrality point. The gap has a width of  $2|\Delta|$  where  $\Delta$  is given in Equation 6.5. The inner two bands are gapped equally, maintaining there degeneracy at the  $\Gamma$  point.

The generation of the band gap is not an artifact of the Born-Oppenheimer approximation. Iadecola and coworkers solved the time dependent Hamiltonian in the low energy limit by absorbing the time dependence of  $\Delta$  in a pseudo spin rotation. The resulting Hamiltonian has the same time independent band gap of  $2|\Delta|$ . The electronic response and system bath coupling are both conserved by this rotation ensuring that the gap could be measured in an electrical transport experiment (Iadecola et al., 2013a). They were additionally able to use this fairly simple system to gain insight into the Floquet formalism used to study more difficult driven solid state systems (Iadecola et al., 2013b).

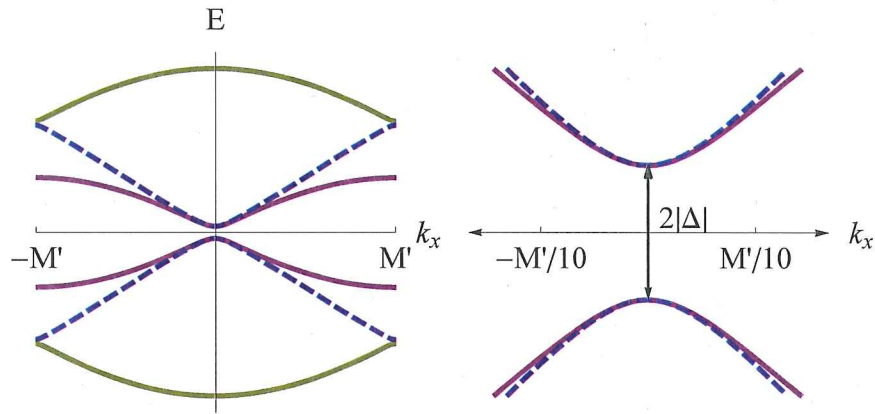


Figure 6.6: The electronic dispersion of the Kekulé lattice along the  $\Gamma$  to  $M'$  direction for a lattice distortion of  $c^*/a = 1\%$ . The plot on the right focuses on the 310 meV energy gap at the  $\Gamma$  point.

The origins of this gapped phase are very similar to the origin of the band gap in polyacetylene. The system is continuously dimerized necessitating an expanded unit cell. Expanding the unit cell requires a shrinking of the BZ and a zone folding of the dispersion. Finally, the lattice modifications induce couplings which open a band gap. The only difference with polyacetylene is that the gap in graphene does not form spontaneously. Instead, phonons must be continuously created to gap the system. *maintain the gap*

## 6.2 Measurement prospects

An experimental measurement of the phonon induced band gap has two components: The excitation of the phonon and the measurement of the resulting band gap. The former is the more difficult of the two; the electrical transport measurements described in Appendix F can be used to measure the resulting band gap. The large momentum

and energy associated with the Kekulé phonon makes their excitation using surface acoustic waves, evanescent fields, surface plasmons, or temperature impractical. In this section we discuss the prospects of directly exciting the Kekulé phonon using a neon seeded helium beam.

To determine the feasibility of this measurement we will estimate the expected band gap. The size of the band gap is estimated in three steps. The band gap is related to atomic displacements, the atomic displacements are related to the number of phonons, and the number of phonons is estimated based on the neon flux and the phonon persistence time. Based on Equation 6.5, the band gap is given by

$$E_g ? \quad \underline{\text{gap}} = 2|\Delta| = 6\beta t_0 \frac{|c|}{a} \approx 50 \text{ eV} \frac{|c|}{a},$$

where  $|c|$  is the amplitude of the phonon oscillation. In a semi-classical approximation  $|c|$  is related to the number of phonons  $N$  through

$$N \frac{1}{2} M \omega^2 |c|^2 = n \hbar \omega \\ \rightarrow |c| = \sqrt{\frac{2\hbar}{M\omega}} \sqrt{\frac{n}{N}} \approx 0.1 \text{ \AA} \sqrt{\frac{n}{N}},$$

where  $n$  is the total number of excited Kekulé phonons in the system,  $N$  is the number of unit cells,  $M$  is the mass of a carbon atom, and  $\omega$  is the frequency of the Kekulé phonon. Thus, the band gap is related to the number of phonons by

$$E_g \quad \underline{\text{gap}} = 6\beta t_0 \sqrt{\frac{2\hbar}{M\omega}} \sqrt{\frac{n}{a^2 N}} \approx 50 \text{ eV} 0.1 \text{ \AA} \sqrt{\frac{n}{A}},$$

where  $a^2 N = A$  is roughly the area of the graphene sheet. Finally, the number of

What illuminated?

in the sample?

in the phonon column length?

excited phonons can be calculated using the steady state solution to the rate equation

$$\frac{dn}{dt} = f\eta A - \frac{n}{\tau} = 0 ,$$

where  $f \approx 10^{18} \text{ atoms/m}^2/\text{s}$  is the neon flux,  $\eta \geq 10^{-2}$  is the scattering efficiency, and  $\tau$  is the persistence time of the phonon. The persistence time is longer than the phonon lifetime because not all phonon decay channels result in fewer phonons. For instance, if a phonon decays into an electron hole pair that electron hole pair can recombine and replace the original phonon. The phonon lifetime can, however, be used to estimate a lower bound for the band gap. For a phonon lifetime of 0.2 ps estimated based on the  $27 \text{ cm}^{-1}$  line width of the Raman 2D feature, the expected band gap is

$$\text{gap} \geq 6\beta t_0 \sqrt{\frac{2\hbar}{M\omega}} \sqrt{f\eta\tau} \approx 50 \text{ eV } 10^{-11} \text{ m } 10 \frac{1}{m} \approx 5 \text{ neV} .$$

This illustrates the difficulty in creating a sufficient number of phonons to open a measurable band gap. If the persistence time were a factor of  $10^{12}$  longer than the phonon lifetime ( $\tau \approx 0.2 \text{ s}$ ), the system would reach a continuous bandgap of roughly 5 meV measurable at room temperature. This seemingly unending lifetime is not entirely outside the range of possibility. Acoustic phonons have lifetimes on this order. A more detailed calculation of the Kekulé phonon decay channels is necessary for a better estimation of the phonon persistence time and the expected band gap.

In the case of short persistence times it makes sense to think of the system stochastically. A neon atom would hit a  $10 \mu\text{m}^2$  sample and create a phonon every  $10 \mu\text{s}$  based on  $f$  and  $\eta$ . If  $\tau \ll 10 \mu\text{s}$  the system would spend most of its time in its unexcited, ungapped, intrinsic state. Assuming that the coherence length of the phonon

covers the whole sample, phonon creation events would cause temporary transitions to a gapped state. For the  $10 \mu m^2$  sample with  $2 \times 10^8$  unit cells, a single phonon excitation would correspond to a band gap of roughly 0.5 meV or 6 Kelvin. Liquid helium temperature electrical transport could be used to measured a gap of this magnitude. However, for a persistence time on the order of picoseconds, the system is only gapped a factor of  $10^{-6}$  of the time. A possible method to overcome this signal to noise issue would be to chop the helium neon excitation beam and lock the electrical transport measurements in to the chopping frequencies.

### 6.3 Summary

The theory behind the phonon induced band gap was developed in the frame work of the Peierls transition. It was shown that exciting the phonon reduces the size of the BZ and couples the  $\mathbf{K}$  and  $\mathbf{K}'$  creating a band gap. The experimental measurement of this exciting physical phenomena is challenging because of the difficulty in exciting a sufficient number of optical phonons.